CFD Letters www.cfdl.issres.net Vol. 4 (4) – December 2012

Finite Difference Based Sigma - Transformation Approach for Liquid Sloshing in a Rectangular Tank under Regular Wave Excitation

Eswaran M[1*] and Ujjwal K. Saha[2,*]

[1] *Structural and Seismic Engineering Section, Reactor Safety Division*
Bhaba Atomic Research Centre, Trombay, Mumbai – 400085, India
[2] *Department of Mechanical Engineering, Indian Institute of Technology Guwahati*
Guwahati -781039, India.

Received: 20/12/2011 – Revised 26/11/2012 – Accepted 02/12/2012

Abstract

In this paper, a fully non-linear finite difference model has been developed based on the inviscid flow equations, and a simple mapping function was used to remove the time-dependence of the free surface in the fluid domain. The time-varying fluid surface is mapped onto a rectangular domain by the Sigma (σ)-transformation. This method is a simple way to simulate non-breaking waves quickly and accurately especially that has a low steepness. The fluid motion is solved in a unit square mesh in the transformed flow domain (i.e., computational domain). Difference between the peaks and troughs of waves are discussed for three different cases of horizontal (surge), vertical (sway) and combined excitations of off and at resonance frequency of the tank. The spectrum analysis of horizontally excited tank is presented. The stability and instability regions associated with vertical and combined excitations conditions are discussed with the plots of free surface elevation, phase-plane diagram and free surface profile.

Keywords: Sloshing; Surge and sway motion; Free surface; Mapping; σ-transformation; Finite difference method.

1. Introduction

The oscillation of the unrestrained free surface of the liquid in a partially filled container due to external excitation is called as sloshing. These motions generate severe hydrodynamic loads that can be dangerous for structural integrity in tanks and will raise the stability problems in rockets, satellites, LNG ships, trucks and even stationary petroleum containers. Free surface of liquid in a container attempts to attain the state of the equilibrium for the effective instantaneous acceleration (gravitational, translational, etc.) felt by the fluid. However, the momentum of the fluid and external forces on the fluid tank will prevent this state of equilibrium. The knowledge of liquid free surface natural frequencies is important in the design of liquid containers subjected to different types of excitation [1, 2]. The dynamic behavior of a free liquid surface depends on the type of excitation

* Corresponding Authors:
[1]Email: eswarm21@gmail.com Telephone: +91 22-25591528
[2]Email: saha@iitg.ernet.in Telephone: +91 361 2582663 Fax: ++ *91 (361) 2690762*
 PII: S2180-1363(12)4173-X

and its frequency content. Civil engineers and seismologists have been studying liquid sloshing effects on large dams, oil tanks and elevated water towers under ground motion.

In 1951 and 1952, Jacobsen and Ayre [3], and Graham and Rodriquez [4] performed some basic studies relevant to this topic. Housner [5, 6] developed an analytical method for the determination of hydrodynamic wall pressures under the assumption that the tank was a rigid structure fixed at the base and only the fundamental sloshing mode was important. Applications in the aerospace industry has been reviewed and discussed by Abramson [7] both analytically and experimentally. Ink-trace experiments were conducted by Cole [8] to study the effect of baffle thickness in the cylindrical tank. In 1970s and in early 1980s, sloshing phenomena in liquid oil carrier vehicles have extensively been studied, since slosh-induced loads can cause serious damage to cargo structure in marine engineering. Externally induced sloshing is studied through interface location technique by Eswaran et *al*., [9]. A lot of researchers have done numerical simulation either by using self made program or by using commercial CFD packages [10-12]. In general, the fluid used in solving the nonlinear sloshing is assumed to be homogeneous, isotropic, viscous and exhibits only limited compressibility. Various models and techniques have been used to solve the problem.

The popular numerical methods like finite difference method, the boundary element method and the finite element method [13] have been used for the sloshing analysis. Behr and Abraham [14] used finite element method to solve the free surface between the inclined walls and explained the difficulties associated with free-surface finite element flow simulations and overcoming techniques. Recently, Sequentially-Coupled Arterial Fluid–Structure Interaction (SCAFSI) technique was proposed by Tezduyar et al. [15] and applied to find the blood pressure profile of the cardiac cycle. The various techniques used to handle the free surface behavior in the sloshing have been the marker and cell (MAC), the volume of fluid (VOF), etc. [16-21]. Recently, Cruchaga *et al.* [22] proposed the 3D remeshing algorithm to avoid the progressive distortion in the distribution of markers in the domain. Recently, the coordinate transformation technique is also applied to this type of problem etc. The particular type of coordinate transformation (stretching on vertical direction) is called σ-transformation. Since they all require complex computer programming in order to treat the time varying free surface boundary and update the computational mesh, the σ-transformation gains popularity because of its simplicity. The σ-transformation was applied to nonlinear steep waves in fixed and base excited tanks by Chern et al. [23] and the waves in relatively deep water was simulated by Turnbull *et al.* [24]. Frandsen [25] investigated numerically steep free surface sloshing in fixed and base-excited rectangular tanks with a focus on moving liquid tank with horizontal and vertical excitations. Recently, Chen and Nokes [26], and Dai and Xu [27] applied σ-transformation to predict the sloshing effects on horizontal cylindrical container and 2D rectangular tank, respectively. The first few sloshing frequencies in a vertically accelerated container have been reported by Eswaran and Saha [28, 29]. Originally, σ- transformation was proposed for meteorological forecasting by Phillips [30]. Later, Blumberg and Mellor [31] and Mellor and Blumberg [32] applied in the context of oceanic and coastal flows.

In this paper, a fully non-linear model for idealized 2-D waves in a numerical wave tank has been developed. The σ-transformation technique is used to capture the liquid free surface which is used to map the asymmetric liquid domain onto a rectangle, such that the moving free surface in the physical plane becomes a fixed line in the computational mapped domain. The fourth order central difference scheme and the Gauss–Seidel point successive over-relaxation iterative procedure are used to capture the free surface wave profiles and free surface elevation plots of the fluid domain. Liquid in a rectangular tank under different regular wave excitations (say horizontal, vertical and combined excited conditions) is studied in detail. Spectrum analysis of horizontal excited tank; and the stable and unstable conditions of vertical and combined motions are also discussed. Section 2 is focused on the mathematical formulations of the present work. Section 3 presents the Mapping procedure which transfers the physical domain to the computational domain. In section 4, the finite

difference discritization of the computational domain is presented. The grid independence study and the behavior of the liquid free surface in fixed tank is studied and discussed in section 5.1 – 5.2. The free surface elevation of liquid, phase plane diagram, spectrum analysis for horizontal excitation is discussed in section 5.3. The stability and instability regions of vertically excited and combined motions (horizontally and vertically) of the tank which will create the interesting fluid free surface behavior is discussed in section 5.4 and 5.5. Additionally, in section 5.5, the free surface profiles for different time intervals and the 3 dimensional surface plots are also showed to explain the severity of the combined motions.

2. Numerical details

A rectangular Cartesian coordinate system is first employed, with origin at the mean free-surface at the left-hand side of the tank. A 2-D nonlinear wave problem is considered in this case, as depicted in Figure 1, where ζ is the free-surface elevation above still water level, b is the length of the tank, and h_s is the still water depth. The fluid in the tank is assumed to be inviscid and irrotational. On the above assumption that the fluid is governed by potential flow theory, the velocity potential ϕ satisfies the Laplace equation. The velocity components normal to the fixed boundaries are zero by definition. The left, the right and the bottom boundary conditions are indicated by L, R, and B, respectively (Figure 1).

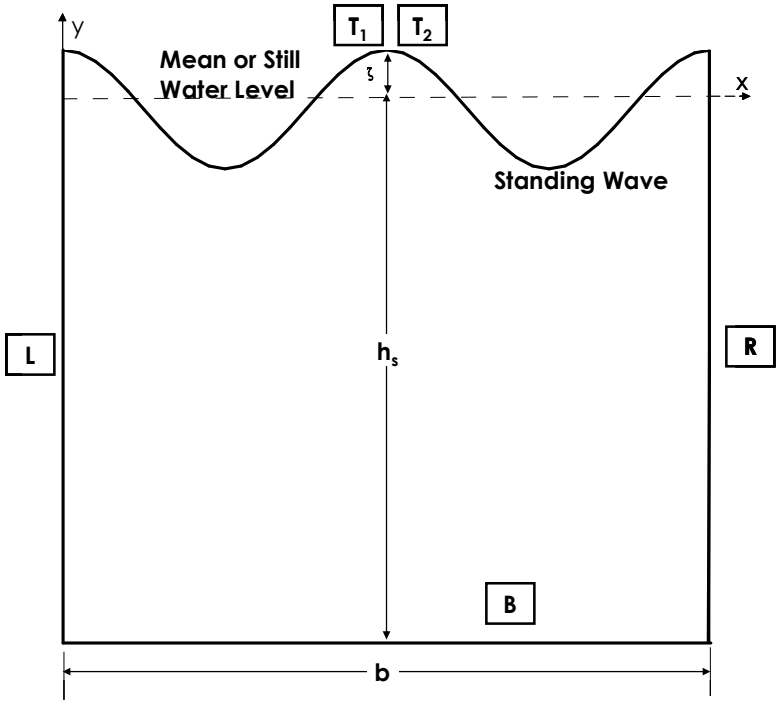

Figure 1. Physical domain

The free surfaces occur at the interface between two fluids. Such interfaces require two boundary conditions to be applied, viz., (i) a kinematic condition that relates the motion of the free interface to the fluid velocities at the free surface (i.e., T1) and (ii) a dynamic condition which is concerned with the force balance at the free surface (i.e., T2). Tanks are studied satisfying the condition that velocity at the bottom and at the side walls is zero. Zero pressure at the free surface of the fluid is also considered in the analysis. In view of the fact mentioned above, kinematic and dynamic conditions must be satisfied on the free surface. Therefore, the boundary conditions for the physical domain are given by,

$$\frac{\partial^2\phi}{\partial x^2}+\frac{\partial^2\phi}{\partial y^2}=0 \quad \text{in the fluid domain} \tag{1}$$

$$\frac{\partial\phi}{\partial n}=0 \quad \text{on the side walls} \tag{2}$$

$$\frac{\partial\zeta}{\partial t}+\frac{\partial\phi}{\partial x}\frac{\partial\zeta}{\partial x}=\frac{\partial\phi}{\partial y} \quad \text{on the free surface} \tag{3}$$

$$\frac{\partial\phi}{\partial t}+\frac{1}{2}\nabla\phi.\nabla\phi+(g+\ddot{Y}_t)\zeta=0 \quad \text{on the free surface} \tag{4}$$

Here, $\ddot{Y}_t$ is the acceleration of the container in the vertical direction which can be neglected from the free surface dynamic boundary condition for fixed container analysis.

The following quantities are introduced for generating dimensionless governing equations for the present study,

$$x'=\frac{x}{b};\quad y'=\frac{y}{b};\quad \zeta'=\frac{\zeta}{A};\quad \ddot{Y}_t'=\frac{\ddot{Y}_t}{g};\quad t'=\sqrt{\frac{g}{b}}t;\quad \phi'=\frac{1}{A\sqrt{bg}}\phi \tag{5}$$

where, g is the acceleration due to gravity, A is the wave amplitude, $\ddot{Y}_t$ is the acceleration of the container and t is the time. Here $x', y', \zeta', \ddot{Y}_t', t'$ and ϕ' represent the dimensionless quantities. Using Eq. (5) (hereafter, primes are omitted for simplification), the non-dimensional governing equation and boundary conditions can be written as follows,

$$\frac{\partial^2\phi}{\partial x^2}+\frac{\partial^2\phi}{\partial y^2}=0 \tag{6}$$

L: $$\frac{\partial\phi}{\partial x}=0 \quad \text{on} \quad x = 0 \tag{7}$$

R: $$\frac{\partial\phi}{\partial x}=0 \quad \text{on} \quad x = b \tag{8}$$

B: $$\frac{\partial\phi}{\partial y}=0 \quad \text{on} \quad y = - h_s \tag{9}$$

T1: $$\frac{\partial\zeta}{\partial t}+E_b\frac{\partial\phi}{\partial x}\frac{\partial\zeta}{\partial x}=\frac{\partial\phi}{\partial y} \quad \text{on} \quad y=\zeta \tag{10}$$

T2: $$\frac{\partial\phi}{\partial t}+E_b\frac{1}{2}\nabla\phi.\nabla\phi+(1+\ddot{Y}_t)\zeta=0 \quad \text{on} \quad y=\zeta \tag{11}$$

where E_b is the amplitude-length ratio ($=A/b$). The Eqns. (6) through (11) form an initial boundary value problem which is the Laplace equation with non-linear boundary conditions imposed on the free surface. Here, the non-linearity is significant for two reasons. Primarily, the elevation of the moving free surface is not known a priori at any given time instant and secondly, the boundary conditions on the free surface [i.e., Eqns. (10) and (11)] contain second order differential terms.

3. Mapping procedure

The time-varying liquid free surface can be mapped onto a fixed plane surface by the proper coordinate transformations, called the σ-transformation, which prevents the need for free surface smoothing for the cases considered herein. In this paper, σ- transformation is applied in the horizontal direction which stretches between the left and the right wall and in the vertical direction which stretches between the moving liquid free surface and the bottom of the liquid container to convert the moving free-surface physical domain onto a fixed square computational domain. The

following section discusses transformation technique in 2-D and 3-D containers elaborately. During transformation, the governing equation and boundary conditions will change appropriately.

3.1. Transformation of 2-D Rectangular Container

Initially, formulations are developed for the fixed container condition, so the horizontal and vertical excitation terms are neglected from the Eq. 4 in the following formulation part.

3.2. Coordinate Transformation

The first transformation adopts the σ-transformation technique to map the liquid domain onto a rectangle, such that the moving free surface in the physical plane (Figure 2) becomes a fixed horizontal line in the σ-transformed domain (Figure 3). The mapping function $\sigma(x,t)$ is defined as

$$\sigma = \frac{y + h_s}{h}, \tag{12}$$

where $$h(x,t) = E_b \zeta(x,t) + h_s, \tag{13}$$

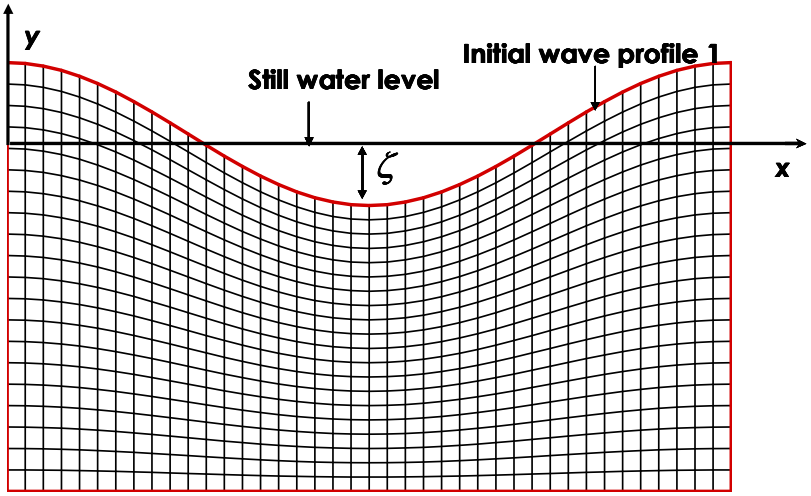

Figure 2. The 2-D Physical domain

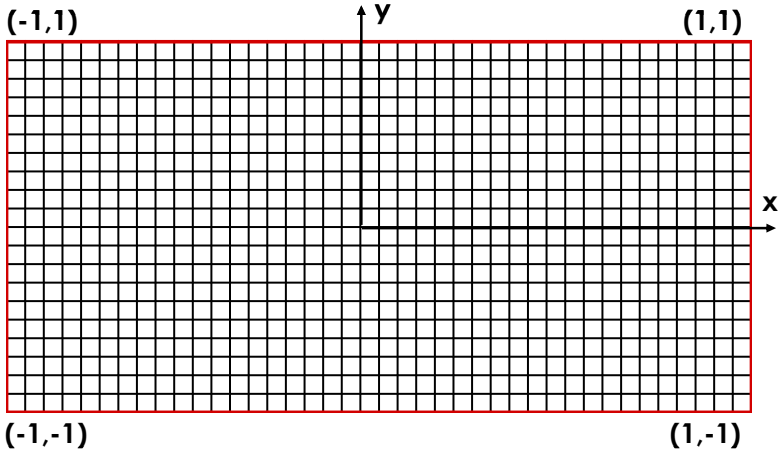

Figure 3. The 2-D Computational domain

Here, $\sigma(x,t)$ is the stretching factor, which varies from 0 to 1. The value of σ at the bottom of the container is *0*, while at the free surface is *1*. The first-order derivatives of σ can be calculated as follows:

$$\frac{\partial\sigma}{\partial t}=\frac{\partial}{\partial t}\left(\frac{y+h_s}{h}\right)=-E_b\frac{\sigma}{h}\frac{\partial\zeta}{\partial t} \quad \text{and} \quad \frac{\partial\sigma}{\partial x}=-E_b\frac{\sigma}{h}\frac{\partial\zeta}{\partial x}. \tag{14}$$

The potential function $\phi(x,y,t)$ in the physical domain is transformed to the potential function $\Phi(X,\sigma,T)$ in the σ-transformed domain.

$x\leftrightarrow X$, $X=2x-1$; $y\leftrightarrow Y$, $Y=2\sigma-1$; and $t\leftrightarrow T$, $T=t$; (15)

Using the chain rule, the first set of derivatives of ϕ with respect to *x, y* and *t* gets transformed as

$$\frac{\partial\phi}{\partial x}=2\frac{\partial\Phi}{\partial X}-E_b\frac{4\sigma}{h}\frac{\partial\zeta}{\partial X}\frac{\partial\Phi}{\partial Y} \tag{16}$$

$$\frac{\partial\phi}{\partial y}=\frac{2}{h}\frac{\partial\Phi}{\partial Y} \tag{17}$$

$$\text{and } \frac{\partial\phi}{\partial t}=\frac{\partial\Phi}{\partial T}-E_b\frac{\sigma}{h}\frac{\partial\zeta}{\partial T}\frac{\partial\Phi}{\partial\sigma} \tag{18}$$

The second set of derivatives of ϕ with respect to *x* and *y* gets transformed as,

$$\frac{\partial^2\phi}{\partial x^2}=4\frac{\partial^2\Phi}{\partial X^2}+l_1\frac{\partial^2\Phi}{\partial Y^2}-l_2\frac{\partial^2\Phi}{\partial X\partial Y}+l_3\frac{\partial\Phi}{\partial Y} \tag{19}$$

$$\frac{\partial^2\phi}{\partial y^2}=\frac{4}{h^2}\frac{\partial^2\Phi}{\partial Y^2} \tag{20}$$

where, $l_1=\left(\frac{4\sigma}{h}\frac{\partial h}{\partial X}\right)^2$; $l_2=\left[\frac{8\sigma}{h}\frac{\partial h}{\partial X}\right]$; $l_3=\left[\sigma\left(\frac{4}{h}\frac{\partial h}{\partial X}\right)^2-\frac{8\sigma}{h}\frac{\partial^2 h}{\partial X^2}\right]$.

Hence, by using the σ-transformation, we can derive the new governing equation and boundary conditions specified on the rectangular σ-transformed domain. The governing equation after the first coordinate transformation is given as:

$$\frac{\partial^2\Phi}{\partial X^2}+L_1\frac{\partial\Phi}{\partial Y}-L_2\frac{\partial^2\Phi}{\partial X\partial Y}+L_3\frac{\partial^2\Phi}{\partial Y^2}=0 \tag{21}$$

$$\text{where, } L_1=\left[\frac{4\sigma}{h^2}\left(\frac{\partial h}{\partial X}\right)^2-\frac{2\sigma}{h}\frac{\partial^2 h}{\partial X^2}\right];\ L_2=2\frac{\sigma}{h}\frac{\partial h}{\partial X};\ L_3=\left[\frac{1}{h^2}+\left(\frac{2\sigma}{h}\frac{\partial h}{\partial X}\right)^2\right] \tag{22}$$

Boundary conditions after the first coordinate transformation are given as:

$$\text{L:}\quad \frac{\partial\Phi}{\partial X}-\frac{2\sigma}{h}\frac{\partial h}{\partial X}\frac{\partial\Phi}{\partial Y}=0 \quad \text{on} \quad X=-1 \tag{23}$$

$$\text{R:}\quad \frac{\partial\Phi}{\partial X}-\frac{2\sigma}{h}\frac{\partial h}{\partial X}\frac{\partial\Phi}{\partial Y}=0 \quad \text{on} \quad X=+1 \tag{24}$$

$$\text{B:}\quad \frac{\partial\Phi}{\partial Y}=0, \quad \text{on} \quad Y=-1 \tag{25}$$

$$\text{T1:}\quad \frac{\partial\zeta}{\partial T}=\left[\frac{2}{h}+\frac{8E_b\sigma}{h}\left(\frac{\partial\zeta}{\partial x}\right)^2\right]\frac{\partial\Phi}{\partial Y}-4E_b\frac{\partial\Phi}{\partial X}\frac{\partial\zeta}{\partial X} \quad \text{on } Y=+1 \tag{26}$$

$$\text{T2:}\quad \frac{\partial\Phi}{\partial T}=M_1\frac{\partial\Phi}{\partial Y}-2E_b\left[\left(\frac{\partial\Phi}{\partial X}-M_2\frac{\partial\Phi}{\partial Y}\right)^2+\left(\frac{1}{h}\frac{\partial\Phi}{\partial Y}\right)^2\right]-(1+\ddot{Y}_t)\zeta \text{ , on } Y=+1 \tag{27}$$

where, $M_1 = \frac{2\sigma}{h}\frac{\partial h}{\partial T}$; $M_2 = \frac{2\sigma}{h}\frac{\partial h}{\partial X}$. (28)

4. Finite difference discretization in the computational plane

In the current study, the finite difference method is adopted. Assuming the transformed domain to be rectangular and constructing on it a unit square mesh of uniform grid in ξ and η directions respectively, the standard fourth order central difference approximation is given by

$$\delta_\xi{}^2 = \frac{-\varphi_{i-2,j} + 16\varphi_{i-1,j} - 30\varphi_{i.j} + 16\varphi_{i+1,j} - \varphi_{i+2,j}}{12(\Delta\xi^2)} + O(\xi^4) \quad (29)$$

$$\delta_\xi \delta_\eta = \frac{1}{2\Delta\xi}\left(\frac{\varphi_{i+1,j+1} - \varphi_{i+1,j-1}}{2(\Delta\eta)} - \frac{\varphi_{i-1,j+1} - \varphi_{i-1,j-1}}{2(\Delta\eta)}\right) + O(\xi^2, \eta^2) \quad (30)$$

where $\varphi(i,j)$ denotes $\varphi(\xi_i, \eta_j)$; $\delta_\xi, \delta_\xi{}^2$ and $\delta_\eta, \delta_\eta{}^2$ are the first and second order central difference operators along ξ and η directions respectively, and $\delta_\xi\delta_\eta$ is the mixed second order central difference operator. Next to the boundary lines are discretized by second order discretization. All the boundary equations are explicitly discretized. The discretized algebraic governing and boundary equations are solved by Gauss–Seidel point successive over-relaxation iterative procedure.

5. Results and discussion

In this problem, the initial wave profile is considered as $\zeta(x,t)\big|_{\tau=0} = A\cos(K_n x)$ and $\varphi(\xi,\eta)\big|_{\tau=0} = 0$, where A is the initial wave amplitude, K_n is the wave number $\left(=\frac{n\pi}{b}\right)$ for n^{th} mode number (n = 0, 1, 2, …..), and x is the distance in the horizontal direction. The initial wave steepness defined for fixed tank studies as $E = A\omega_n{}^2 / g$, where gravity field g is usually considered as 9.81 m/s^2. Here, the ratio of h_s to b is considered as 1:2. The linear natural sloshing frequencies in the two dimensional rectangular tank are expressed by

$$\omega_n = \sqrt{K_n g \tanh(K_n h_s)}, \qquad n=1, 2, 3\ldots \quad (31)$$

Now X_D'' and Y_D'' are switched off for fixed tank condition in dynamic boundary condition. Two quantities are usually kept in mind in the sloshing studies: the amplitude of the wave and the excitation frequency. Here, the amplitude is measured by the wave steepness. The relation between the acceleration and wave steepness is discussed above.

5.1. Independence Study

In order to display that the solution is grid and time independent, simulations have been performed using different numbers of grid nodes and different values of Δt as shown in Figures 4 and 5.

The wave profiles along the tank at three different times for the first sloshing mode (n=2) are plotted. Results for different grid resolutions are shown related to moderate a wave amplitude (E=0.0338) for time steps of $\Delta t = 0.003$ sec. Figure 4 shows the different grid size of 21×21,

41×21, 41×41 and 41×61. Initially, grid size is increased in the horizontal direction from 21 to 41. As it is a fixed boundary, it is found that there is not much variation on horizontal direction, and then, the grid points are increased from 21 to 41 and 61 in vertical direction. Increasing the grid points in the vertical direction is found to be more effective in improving the accuracy than increasing the grid points in the horizontal direction since it has the moving boundary at top. It has been found that a grid size of 41×61 and 41×41 and a time step of 0.003 sec and 0.004 sec provided sufficient accuracy to capture nonlinearities related to steep wave predictions (E > 0.02). There is not much variation in vertical direction above the grid size of 41×41 for moderate wave steepness, and therefore, the grid size of 41×41 is sufficient for this problem.

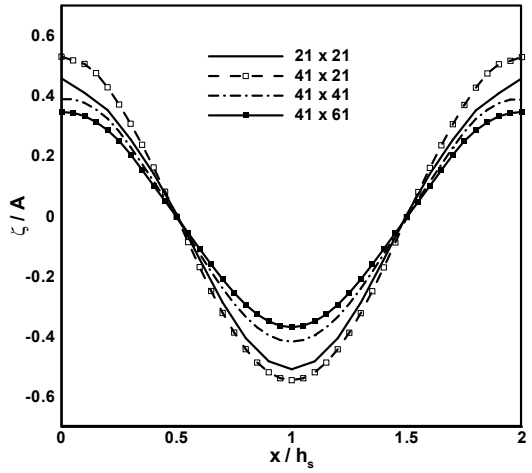

Figure 4. Grid independence study for E=0.033 at time 7.5 sec.

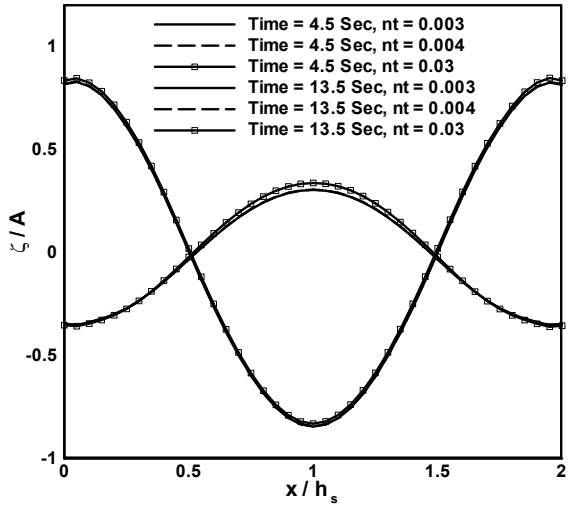

Figure 5. Time independence study for E=0.033 and grid size 41×61.

5.2. Effect of Wave Steepness in Fixed Tank

The wave characteristics include a crest at the top and a trough at the bottom. The difference in elevation between the crests and trough is the wave height. The distance between the adjacent crests or the troughs of wave is termed the wavelength. The ratio of wave height to wavelength is the wave's steepness. While increasing the wave steepness the nonlinearity increases. The free surface elevations at the left wall, in the middle and at right wall of the tank are showed in Figure 6 (a) and 6 (c). When wave steepness increases, the considerable changes

have been observed in the free surface wave profile. On the other hand, the wave phase plane diagrams are shown in Figures 6 (b) and 6 (d). These profiles are a repeatable pattern which is observed at left wall of the tank. The wave phase plane diagram for low steepness is almost a perfect circle as seen from Figure 6(b), while at the same time, increasing the steepness makes the phase plane diagram to become oval as depicted in 6 (d).

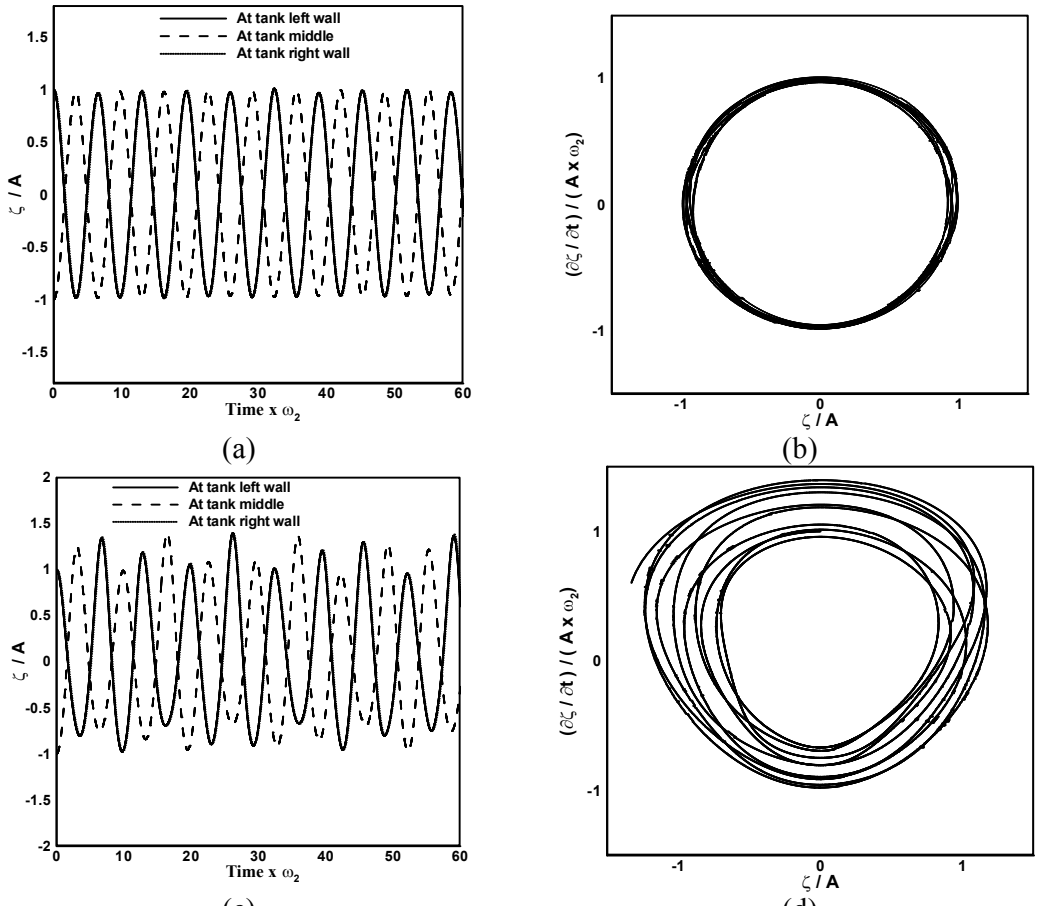

Figure 6. Fixed tank elevation and phase plane diagram for n=2 with grid size 41×61 and $\Delta t = 0.003$ sec: (a) - (b) E=0.0338; (c) - (d) E=0.338.

5.3. Horizontally Excited Tanks

For the horizontally excited tank condition, Y_D'' was switched off from the dynamic boundary condition at top wall. The horizontal excited acceleration is fixed as $X_D'' = (-\omega_h A_h \cos(\omega_h t))$. When the external horizontal forcing frequency is equal to the natural sloshing frequency of the liquid, the resonance will occur. In this section, the free surface motions are numerically examined off- and at resonance conditions. The initial wave profile is considered as $\varphi(\xi,\eta)\big|_{\tau=0} = 0$. For initial wave impulse is considered as $\zeta(x,t)\big|_{\tau=0} = A\cos(K_n x)$ and for zero impulse condition is $\zeta(x,t)\big|_{\tau=0} = 0$. And K_h is the measure of nonlinearity parameter which is calculated from $k_h = \dfrac{A_h \omega_h{}^2}{g}$, where A_h is the excitation amplitude. The sloshing motion is more violent at the natural frequency of the container when the excitation frequency is equal to the first mode rather than at the third mode, which is a well-known resonance phenomenon.

5.3.1. *Off and at resonance of horizontally excited tanks*

The horizontal frequency ratio $\Omega_x \left(= \frac{\omega_h}{\omega_n} \right)$ is speckled as 0.7, 0.9 and 1.3 for off-resonance and 1 for at resonance conditions. To validate the developed model, the present data have been compared with the results of Frandsen [25]. The results have been found to be in good agreement as seen from Figure 7(a). While increasing the excitation frequency, some interesting free surface elevation shapes are observed (Figures 7a, 7c, 8a and 9a). When the frequency ratio Ω_x is small, standing waves are observed upto certain level. Then waves are variations in waves are aroused slowly as shown in Figure 7(a) and while we come around Ω_x = 0.8 to 0.9 the waves are showing the complete different elevation patterns which has the cunning points at certain intervals.

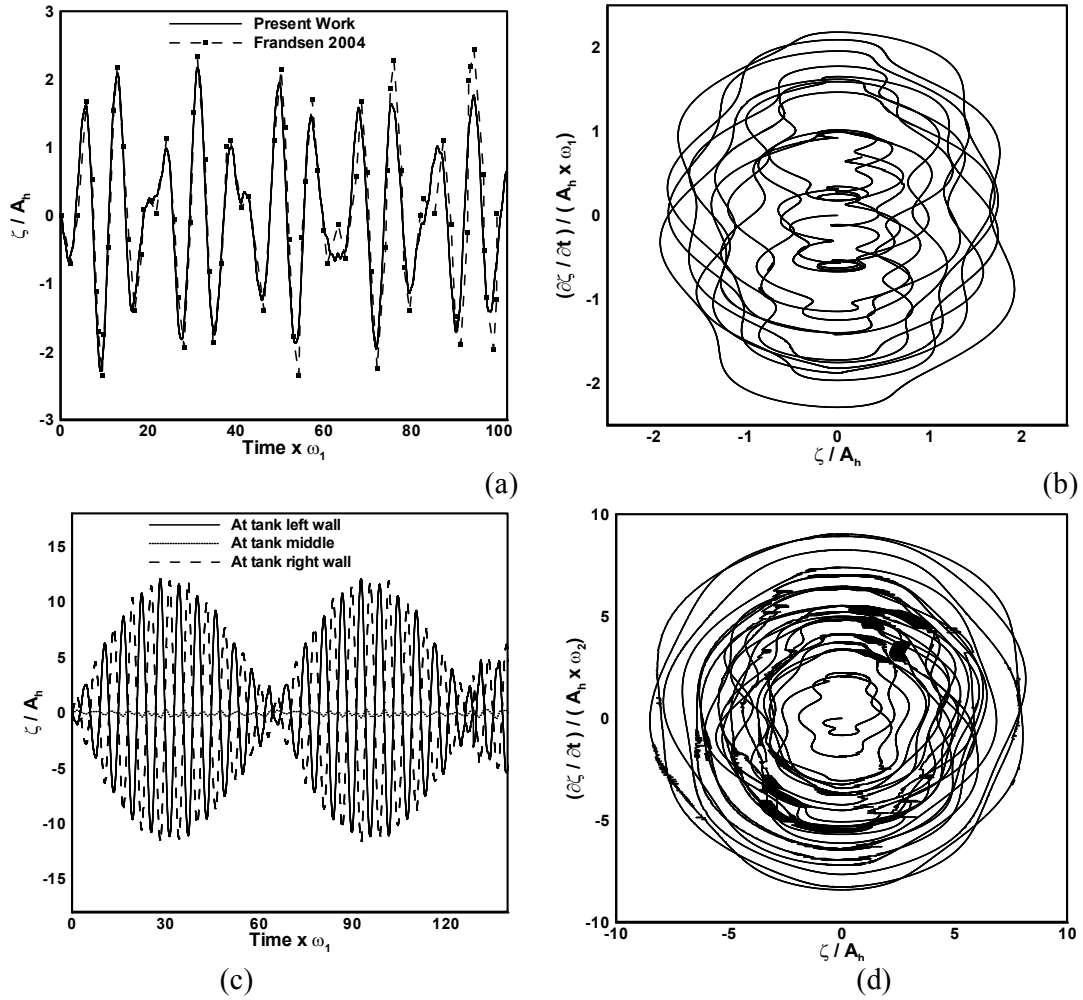

Figure 7. Off-resonance horizontal excited tank elevation and phase plane diagram for n=1 with grid size 41×61 K_h=0.0034 and $\Delta t = 0.003$ sec (a) - (b) $\Omega_x = 0.7$ and (c) - (d) $\Omega_x = 0.9$

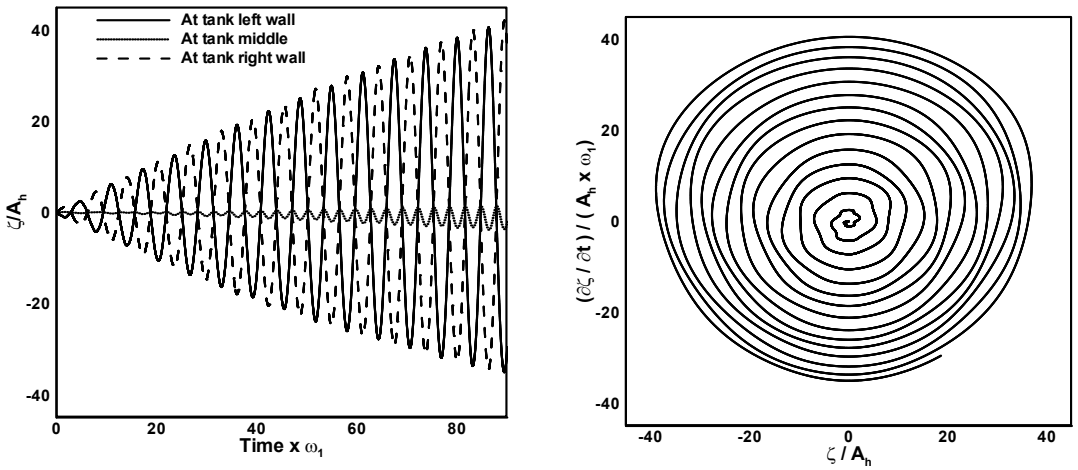

(a) (b)

Figure 8. At resonance conditions horizontal excited tank elevation and phase plane diagram for n=1 with grid size 41×61 K_h=0.0034 and $\Delta t = 0.003$ sec.

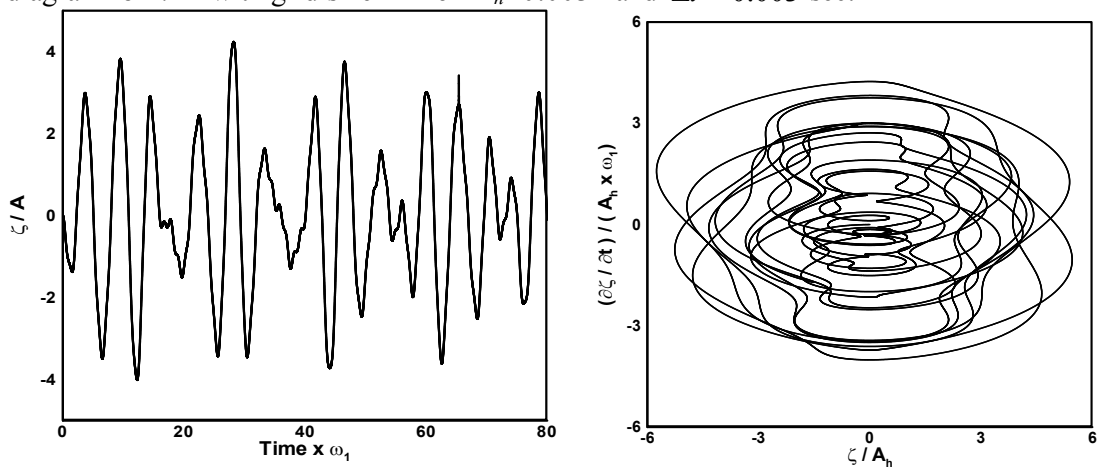

(a) (b)

Figure 9. Off-resonance horizontal excited tank elevation and phase plane diagram for n=1 with grid size 41×61, K_h=0.0034 and $\Delta t = 0.003$ sec $\Omega_x = 1.3$

After reaching the Ω_x=1 the free surface elevation are growing continuously with constant increments (Figure 8). Since, at this point the excitation frequency is matched with system natural frequency. Figure 8 (a) showed as the free surface elevation is observed 36 times to amplitude of excitation approximately at non-dimensional time 80. As discussed in section 5.3, in Figure 8(a), free surface elevation is shown with two initial conditions viz. zero impulse and initial impulse. After few seconds, both the results match very closely. It is observed that the initial impulse has not undergone much variation from the original behaviour of the liquid wave profiles during sloshing. However, at low frequencies, one can expect very small deviations between the initial impulse and the zero impulse. Finally, the frequency ratio was increased to Ω_x = 1.3, where by the free surface elevation drastically reduces to 3.4 times (from 36 times at resonance frequency) to the excitation amplitude approximately at non-dimensional time 80. Figures 7(b), 7(d), 8(b) and 9(b) show the phase plane diagram for their respective frequencies. In Figure 8(b), the phase plane diagram is moving in a circular path and finally it attains the spiral shape, since it is drawn at the resonance condition.

5.3.2. *Spectrum analysis for horizontally excited tanks*

The Fast Fourier Transform (FFT) is extremely important in the area of frequency (spectrum) analysis because it takes a discrete signal in the time domain and transforms that signal into its discrete frequency domain representation. The FFT does not directly give the spectrum of a signal. The Shift is required for visualizing the Fourier transform with the zero-frequency component in the middle of the spectrum.

The spectra of a wave elevation are computed by the FFT, which is given by

$$X(K) = \sum_{j=1}^{N} x(j)\omega_N^{(j-1)(k-1)}, \tag{32}$$

where $\omega_n = e^{(-2\pi i)} / N$, is a N^{th} root of unity. In order to avoid the effect of discontinuity at the boundary, the hamming window as given by

$$\omega(n) = 0.54 - 0.46\cos\left(2\pi \frac{n}{N}\right), 0 \le n \le N \tag{33}$$

is used, where the window length is $L=N+1$. Figure 10 shows the spectra of wave elevations at the tank left corner. It also caused peaks in the power spectra to become bigger and more peaks appear at different frequencies. Figure 10 (a) shows that the maximum spectral peak occurs at the excitation frequency when the excitation frequency is less than the first natural frequency and a secondary peak occurs at the container natural frequency. While frequency ratio Ω_x approaches 0.9, the partial merging of first mode frequency and the excitation frequency slightly increase the energy of the signal as shown in Figure 10 (b). In Figure 10 (c), a single peak of the dimensionless sloshing energy is observed at frequency ratio of 1, which is irrespective of the magnitude of the excitation frequency. At the first modal frequency, the response component is observed to increase as the frequency increases. When the excitation frequency is greater than ω_1, the domination of the first mode reduces with an increase in the frequency ratio. When the excitation frequency is greater than the first mode (Figure 10 d), the sloshing dominates at the first modal frequency up to second mode ($\omega_2 = 1.5\,\omega_1$) and till this frequency, the secondary peak is observed at the excitation frequency as can be seen in Figure 10 (d).

5.3.3. Vertically excited tanks

The initial conditions for vertical excited tank are same as the sloshing motion simulation of the fixed tank. It is difficult to simulate sloshing only with vertical excitation by experiments. In order to have an initial perturbation in the free surface inside the container, horizontal motions need to be excited before the vertical excitation. To avoid this situation, the initial standing wave profile is assumed for this work. Initial wave impulse is required for vertically excited condition and it is considered here as $\zeta(x,t)\big|_{\tau=0} = A\cos(K_n x)$. The vertical acceleration of tank is given by $Y_D'' = (-\omega_v A_v \cos(\omega_v t))$, where A_v is the vertical forcing amplitude, t is the time, ω_v is the angular frequency of forced vertical motion. The horizontally excited tank acceleration term X_D'' is switched off from the dynamic boundary condition at top wall for this analysis. The initial velocity potential in the fluid domain is considered as $\varphi(\xi,\eta)\big|_{\tau=0} = 0$.

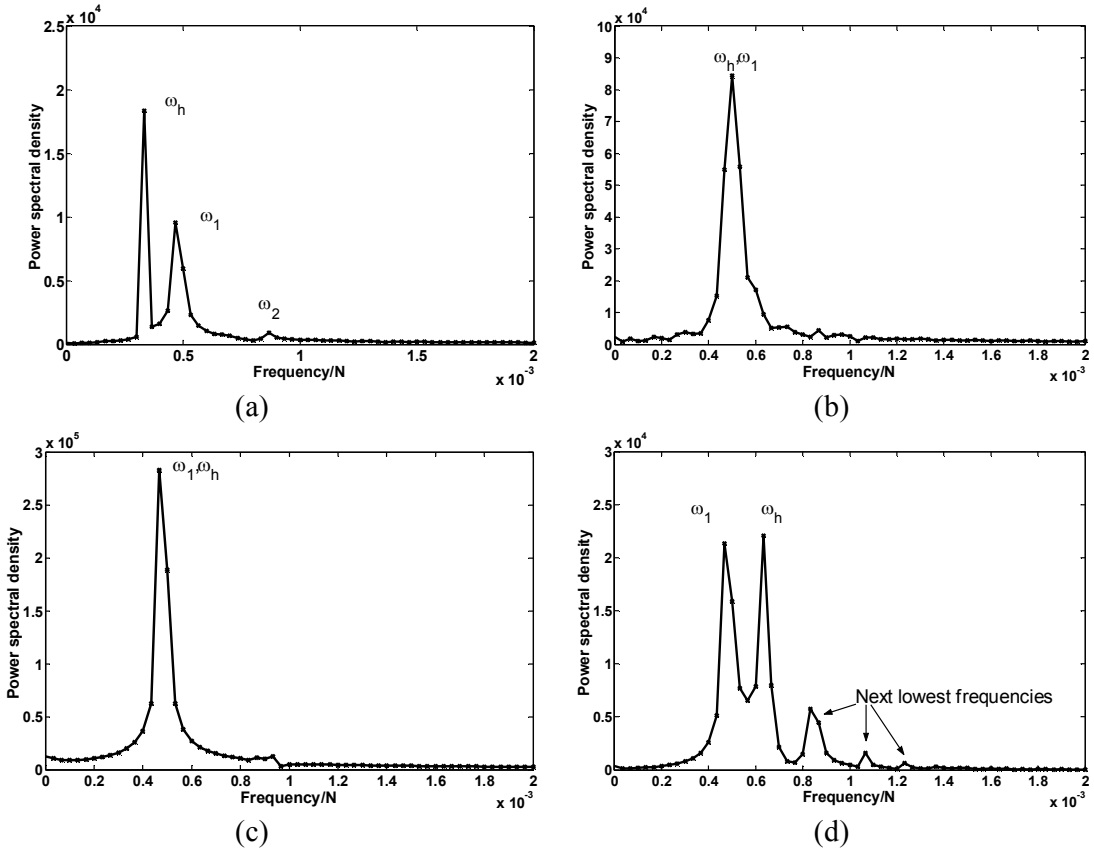

Figure 10. Spectrum analysis for horizontal excited tank off and at resonance frequencies.

The waves generated by the vertical excitation are called Faraday waves as explored originally by Faraday [34] through his experiments. Faraday waves are the resonant waves when the excitation frequency is twice the natural frequency for some initial perturbation in the container. This resonance condition is called parametric resonance. The study dealing with vertical excitation of liquids in a container is referred to as parametric sloshing. For the vertically excited tank, the parameter $k_v = A_v\omega_v^{\,2}/g$ is a measure of the importance of the vertical forcing motion and E is the measure of nonlinearity. Frandsen [25] plotted the instability map between $\Omega_v = \omega_n/\omega_v$ and k_v and discussed results from stability and instability regions. If any of the pairs of the parameters lie in the instability region, then the corresponding mode grows exponentially with time. In this section, the profiles are given with stability and instability region. Figures 11 (a) and (b) are show behaviour of the liquid free surface and phase plane diagrams respectively from the stability region (Ω_v = 1.38 and K_v = 0.4). The unstable regions results from Ω_v = 1 and K_v = 0.4 for elevation and phase plane are plotted in Figures 11 (c) and (d).

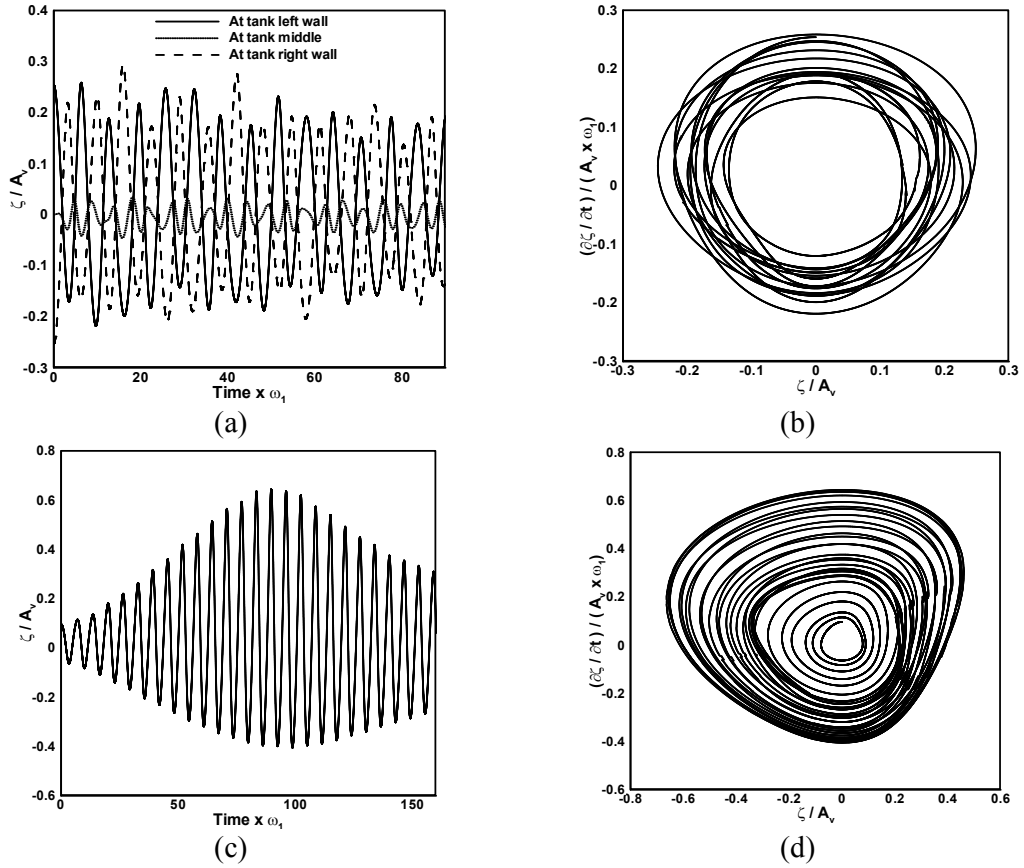

Figure 11. Stable and unstable regions from vertically excited tank elevation and phase plane diagram for n=1 with grid size 41×61 and $\Delta t = 0.003$ sec (a) - (b) Stable solution at $\Omega_v = 1.38$ and $K_v = 0.4$; (c) - (d) Unstable region at $\Omega_v = 1$ and $K_v = 0.4$.

5.3.4. Combined excitation study (Sway and surge motion)

The combined motion of horizontal and vertical excitation is discussed in this section. The vertical excited container is used for an ideal earthquake. And the combined motions of horizontal and vertical excitations are two major considerable motions during earthquake. The water waves at resonance may create the impact pressure rise inside the tanks. When the liquid is striking on the wall, the impact pressure which might have been raised near the critical pressure range of the tank material will cause the structural damage in the tanks. The violent sloshing of combined excitation creates localized high impact loads on the tank roof and walls which may damage the tank. During the combined excitation of tank, the flow behaviour becomes tumultuous which creates the intricate free surface shapes during this type of excitation. Due to the vertical excitation being present with this combined motion, the instability regions exist as discussed in section 5.4. The initial wave impulse is required for vertically excited condition and it is considered here as $\zeta(x,t)\big|_{\tau=0} = A\cos(K_n x)$. The vertical acceleration of tank is $Y_D'' = (-\omega_v A_v \cos(\omega_v t))$ and the horizontal excited acceleration is fixed as $X_D'' = (-\omega_h A_h \cos(\omega_h t))$. The initial velocity potential in the fluid domain is considered as $\varphi(\xi,\eta)\big|_{\tau=0} = 0$. The stable and unstable regions from horizontally and vertically excited tank elevation and phase plane diagram are presented Figure 12 (a) through (d). Figure 12 (a) and (b) are stable solutions from n=1 with

grid size 41×61, $\Delta t = 0.003$ sec, Ω_v= 1.38, Ω_x=0.7 and K_v = 0.4 while Figure 12 (c) and (d) are from unstable region at n=1 with grid size 41×61, $\Delta t = 0.003$ sec, Ω_v= 0.5, Ω_x=0.7 and K_v = 0.4. As discussed, if any of the pairs of the parameters lie in the instability region, then the corresponding mode grows exponentially with time as shown in Figure 12(c) and (d).

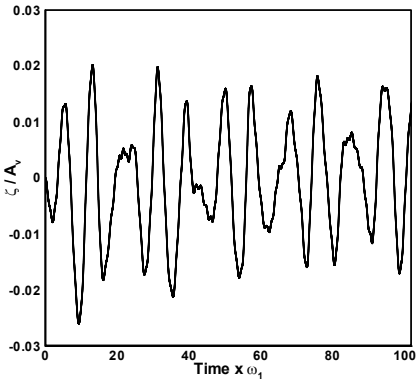

(a) Stable solution at Ω_v = 1.38, Ω_x =0.7 and K_v = 0.4.

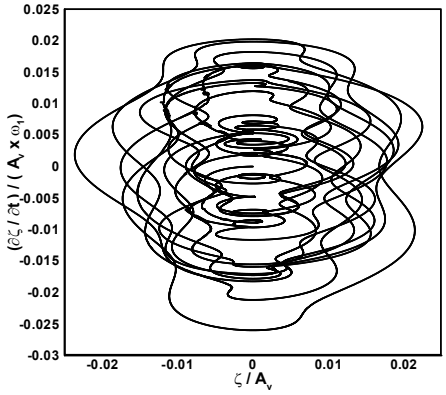

(b) Stable solution at Ω_v = 1.38, Ω_x =0.7 and K_v = 0.4.

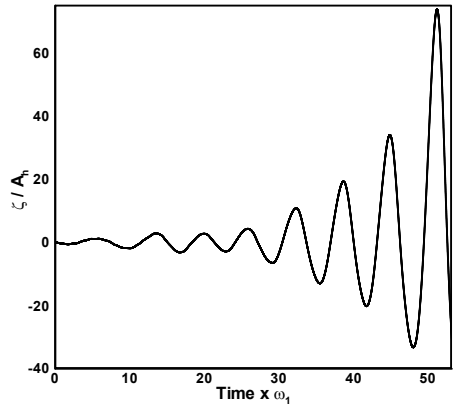

(c) Unstable region at Ω_v = 0.5, Ω_x =0.7 and K_v = 0.4.

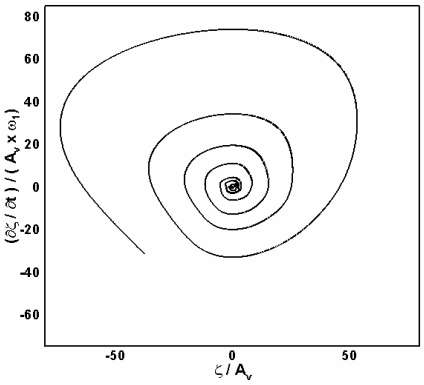

(d) Unstable region at Ω_v = 0.5, Ω_x =0.7 and K_v = 0.4.

Figure 12. Stable and unstable regions from horizontally and vertically excited tank elevation and phase plane diagram for n=1 with grid size 41×61 and $\Delta t = 0.003$ sec.

The stable and unstable region surface plots are shown in Figure 13 (a) and (b). The surface plot is drawn between time and tank width and free surface elevation which is showed in Figure 13 (a) from the stable region (n=1 with grid size 41 × 61, $\Delta t = 0.003$ sec, Ω_v = 1.38, Ω_x =0.7 and K_v = 0.4) and 14(b) from unstable region (n=1 with grid size 41 × 61, $\Delta t = 0.003$ sec, Ω_v = 0.5, Ω_x =0.7 and K_v = 0.4). Figure 14 shows the free surface elevation from time 2.1 sec to 5.4 sec with the time interval of 0.3 seconds. The free surface elevation along the tank width is illustrated here. It is observed that the waves are moving up and down, and it must not be a uniform wave as observed in a fixed tank. One can easily find the considerable variation due to the combined excitation.

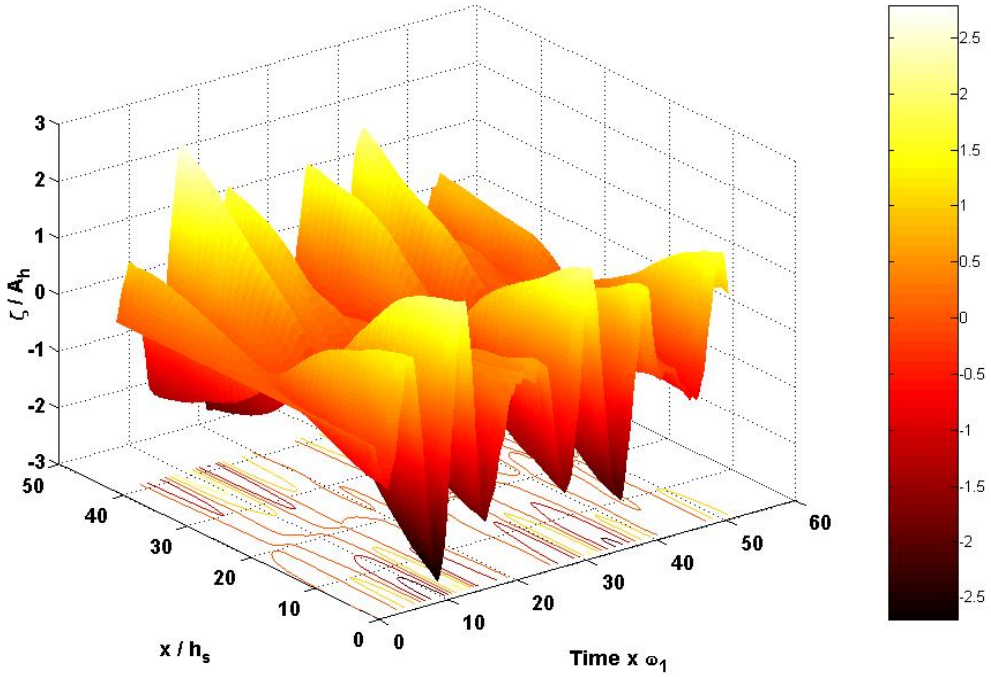

(a) Stable region $\Omega_v = 1.38$ and $K_v = 0.4$

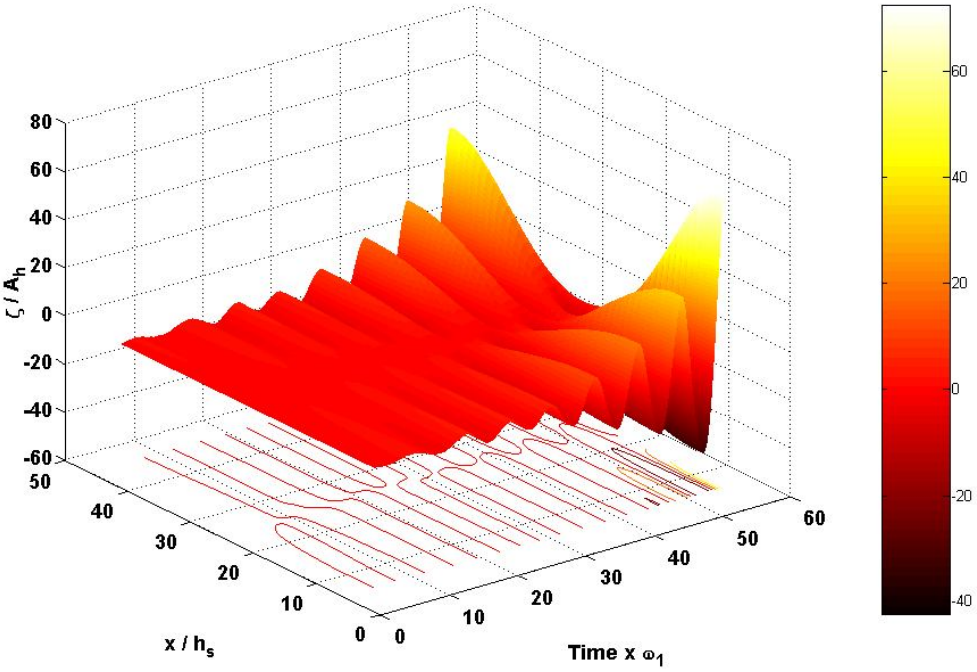

(b) Unstable region $\Omega_v = 0.5$ and $K_v = 0.4$

Figure 13. Stable and unstable regions from horizontally and vertically excited tank surface plot for n=1 with grid size 41×61 and $\Delta t = 0.003$ sec at Ω_x =0.7.

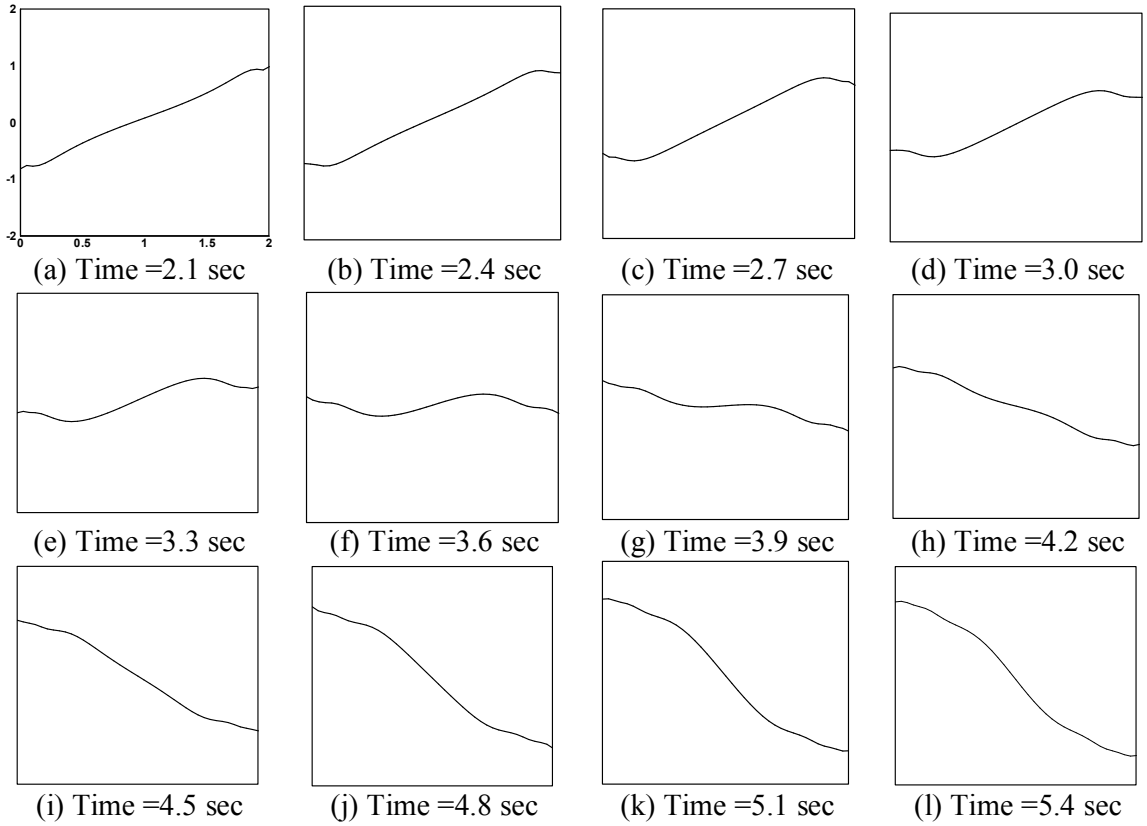

(a) Time =2.1 sec (b) Time =2.4 sec (c) Time =2.7 sec (d) Time =3.0 sec

(e) Time =3.3 sec (f) Time =3.6 sec (g) Time =3.9 sec (h) Time =4.2 sec

(i) Time =4.5 sec (j) Time =4.8 sec (k) Time =5.1 sec (l) Time =5.4 sec

Figure 14. Free surface profile diagram for horizontally and vertically excited tank n=1 with grid size 41×61, $\Delta t = 0.003$ sec, $\Omega_v = 1.38$, Ω_x =0.7 and $K_v = 0.4$.

6. Summary and Conclusions

This paper deals with the non-linear effects of standing wave motion of liquid in a 2-D rectangular tank. Governing equation and boundary conditions have been developed based on the potential flow theory. A fully non-linear finite difference model had been developed based on the inviscid flow equations, and a simple mapping function is used to remove the time-dependence of the free surface in the fluid domain. Mapped governing equations and boundary conditions are solved by finite difference method. Results of liquid sloshing induced by horizontal, vertical and combined (horizontal and vertical) base excitations have been presented for small to steep non-breaking waves. Simulations are limited to water fill ratio (h_s/b) of 0.5. However, this numerical model is valid for any water depth except shallow and deep sloshing. For the shallow sloshing, viscous effects would become important, which we considered as inviscid fluid in our numerical model. Primarily, the model was validated for sloshing motions and the effect of the steepness of wave for a fixed tank. The σ-transformation is limited to small steep non overturning waves. The numerical model captured the free surface displacement at the left wall, right wall and at the center of the tank. A good agreement between our numerical model and previously published result [25] had been obtained for low steeping waves. The grid independent test was conducted for grid sizes of 21×21, 41×21, 41×41 and 41×61 and finally, 41×61 is selected as grid resolution. Increasing grid points in the vertical direction was found to be more effective in improving the accuracy. The wave profiles along the tank at three different times for the first sloshing mode were plotted. Phase-plane plot shows the behaviour of the free surface with repeatable patterns for the peaks and troughs in bounded orbits.

The numerical wave tank captured steep waves generated by horizontal, vertical and combined forcing amplitudes. The horizontally excited tank free surface elevation and phase plane diagram was discussed with off and at resonance frequencies. Behaviours show the effect of wave excitation while matching with resonance frequency. The spectrum analysis of horizontally excited tank is also presented. The vertical and excitation causes the instability associated with parametric resonance of the combined motion for a certain set of frequencies and amplitude of the vertical motion. The initial condition for the surface elevation was an important parameter as there should be some initial perturbation in the system for the generation of waves due to vertical excitation. These conditions were also applied to combined excitation. Here, the data were chosen from the stability region as well as instability region as discussed in section 5.4 and 5.5. Early simulations of the liquid sloshing problem have mostly been performed with waves of small steepness. But the present work reported with low and moderate steepness of wave. The present work can be extended to a 3D tank and can also be solved by some other higher order numerical methods like compact scheme. Moreover, σ -transformation can be applicable for polar coordinates geometries as well.

Nomenclature

A	Wave amplitude, *m*
A_v	Vertical forcing amplitude, *m*
A_x	Horizontal forcing amplitude, *m*
b	Length of the tank, *m*
E	Wave steepness
h_s	Still water depth, *m*
h	Instant water height from tank bottom, *m*
K_n	Wave number
K_v	Nonlinearity parameter in vertical direction
K_h	Nonlinearity parameter in horizontal direction
n	Mode number
Y_D''	Vertical acceleration of the tank, m/s^2
X_D''	Horizontal acceleration of the tank, m/s^2
Greek symbols	
ω_n	Natural sloshing frequency , *rad/s*
ω_v	Frequency of vertical motion, *rad/s*
ω_h	Frequency of horizontal motion, *rad/s*
ζ	Free-surface elevation, *m*
σ	Stretching Factor
ϕ	Velocity potential function at physical domain (x, y, t)
Φ	Velocity potential function at transformed domain (X, σ, T)
φ	Velocity potential function at Computational domain (ξ, η, τ)
Ω_v	Frequency ratio in vertical direction $(= \omega_n / \omega_v)$
Ω_x	Frequency ratio in vertical direction $(= \omega_h / \omega_n)$
δ, δ^2	First and second order central difference operators
δ_ξ, δ_η	Mixed second order central difference operator.

References

[1] Maleki, A., and Ziyaeifar, M., *Sloshing damping in cylindrical liquid storage tanks with baffles*. Journal of Sound and Vibration, 2008. **311**: p. 372–385.

[2] Ibrahim, R.A., *Liquid Sloshing Dynamics: Theory and Applications*. 1st edition, Cambridge University Press, 2005, New York.

[3] Jacobsen, L.S., and Ayre, R.S., *Hydrodynamic experiments with rigid cylindrical tanks subjected to transient motions.* Bulletin of the Seismological Society of America, 1951. **41**: p. 313-346.

[4] Graham, E.W., and Rodriguez, A.M., *Characteristics of fuel motion which affect airplane dynamics,* Journal of Applied Mechanics, 1952. **19**: p. 381–388.

[5] Housner, G.W., *Dynamic pressures on accelerated fluid containers*. Bulletin of the Seismological Society of America, 1957. **47**: p. 15-35.

[6] Housner, G.W., *The dynamic behavior of water tanks*. Bulletin of the Seismological Society of America, 1963. **53**: p. 381-387.

[7] Abramson, H.N., *The dynamics of liquids in moving containers*. Report SP 106, 1966, NASA.

[8] Cole, H.A., *Baffle thickness effects in fuel sloshing experiments*. TN D-3716, 1966. NASA.

[9] Eswaran, M., Singh, A., and Saha, U.K., *Experimental measurement of the surface velocity field in an externally induced sloshing tank*, Proceedings of the Institution of Mechanical Engineers, Part M, Journal of Engineering for the Maritime Environment, 2011. **225**(2): p. 133-148.

[10] Modi, V.J., and Seto, M.L., *Suppression of flow-induced oscillations using sloshing liquid dampers: analysis and experiments*. Journal of Wind Engineering and Industrial Aerodynamics, 1997. **67** & **68**: p. 611-625.

[11] Frandsen, J.B., Borthwick, A.G.L., *Simulation of sloshing motions in fixed and vertically excited containers using a 2-D inviscid σ-transformed finite difference solver*. Journal of Fluids and Structures, 2003, **18**: p. 197-214.

[12] Godderidge, B., Turnock, S., Tan, M., Earl, C., *An investigation of multiphase CFD modeling of a lateral sloshing tank*. Computers and Fluids, **38**: p. 183–193.

[13] Cho, J.R., Lee, H.W., *Numerical study on liquid sloshing in baffled tank by nonlinear finite element method*. Computer Methods in Applied Mechanics and Engineering, 2004. p. **193**: 2581–2598.

[14] Behr, M., Abraham, F., *Free-surface flow simulations in the presence of inclined walls.* Computer Methods in Applied Mechanics and Engineering, 2002. **191**: p. 5467–5483.

[15] Tezduyar, T.E., Schwaab, M., and Sathe, S., *Sequentially-coupled arterial fluid–structure interaction (SCAFSI) technique.* Computer Methods in Applied Mechanics and Engineering, 2009. **198**:p. 3524–3533.

[16] Popov, G., Sankar, S., Sankar, T.S., and Vatistas, G.H., *Dynamics of liquid sloshing in horizontal cylindrical road containers.* Proceedings of the Institution of Mechanical Engineers, Part C: Journal of Mechanical Engineering Science, 1993. **207-C6**: p. 399-406.

[17] Akyildiz, H., and Unal, N., *Sloshing in a three-dimensional rectangular tank: numerical simulation and experimental validation.* Ocean Engineering, 2006. **33**: p. 2135–2149.

[18] Cho, J.R., Lee, H.W., and Ha, S.Y., *Finite element analysis of resonant sloshing response in 2D baffled tank.* Journal of Sound Vibration, 2005. **288**: p. 829–845.

[19] Arafa, M., *Finite element analysis of sloshing in rectangular liquid-filled tanks.* Journal of Vibration Control, 2007. **13**: p. 883–903.

[20] Hirt, C.W., and Nichols, B.D., *Volume of fluid (VOF) method for the dynamics of free boundaries.* Journal Computational Physics, 1981. **39**: p. 201–205.

[21] Eswaran, M., Saha, U.K., and Maity, D., *Effect of baffles on a partially filled cubic tank: Numerical simulation and experimental validation*. Computers and Structures, 2009, **87**(3-4): p. 198–205.

[22] Cruchaga, M., Celentano, D., Breitkopf, P., Villon, P., and Rassineux, A., *A surface remeshing technique for a lagrangian description of 3D two-fluid flow problems.* International Journal of Numerical Methods in Fluids, 2010. **63**: p. 415-430.

[23] Chern, M.J., Borthwick, A.G.L., and Taylor, R.E., *A pseudospectral σ-transformation model of 2-D nonlinear waves.* Journal of Fluids and Structures, 1999. **13**: p. 607- 630.

[24] Turnbull, M.S., Borthwick, A.G.L., and Taylor, R.E., *Numerical wave tank based on a σ-transformed finite element inviscid flow solver*. International Journal for Numerical Methods in Fluids, 2003, **42**: p. 641–663.

[25] Frandsen, J.B., *Sloshing in excited tanks.* Journal of Computational Physics, 2004. **196**: p. 53-87.

[26] Chen, B.F., and Nokes, R., *Time-independent finite difference analysis of fully non-linear and viscous fluid sloshing in a rectangular tank.* Journal of Computational Physics, 2005. **209**: p. 47-81.

[27] Dai, L., and Xu, L., *A numerical scheme for dynamic liquid sloshing in horizontal cylindrical containers*. Proceedings of the Institution of Mechanical Engineers, Part D, Journal of Automobile Engineering, 2006. **20**: p. 901-918.

[28] Eswaran, M., and Saha, U.K., *Low steeping waves simulation in a vertical excited container using σ-transformation*. Paper No. OMAE2009–**80248,** 28th International Conference on Ocean, Offshore and Arctic Engineering, 2009, Honolulu, Hawaii, USA.

[29] Eswaran, M., and Saha, U.K., 'Wave simulation in an excited cylindrical tank using sigma transformation', Paper No. IMECE2010-**39752,** ASME International Mechanical Engineering Congress & Exposition, 2010, Vancouver, Canada.

[30] Phillips, N.A., *A coordinate system having some special advantages for numerical forecasting*. Journal of Atmospheric Sciences, 1957, **14**: p.184–185.

[31] Blumberg, A.F., and Mellor, G.L., *A coastal ocean numerical model*, Mathematical Modeling of Estuarine Physics, 1980. P. 203-219.

[32] Mellor, G.L., and Blumberg, A.F., *Modeling vertical and horizontal diffusivities with the sigma coordinate system.* Monthly Weather Review, 1985. **113**: p. 1379-1383.

[33] Faltinsen, O.M., *A nonlinear theory of sloshing in rectangular tanks.* Journal of Ship Research, 1974, **18**: p. 224-241.

[34] Faraday, M., *On a peculiar class of acoustical figures; and on certain forms assumed by groups of particles upon vibration elastic surface.* Philosophical Transactions of the Royal Society, 1831. London **121**: p. 299–340.